Article

Cooling particle-coated bubbles: destabilization beyond dissolution arrest

Vincent Poulichet, and Valeria Garbin

Langmuir, **Just Accepted Manuscript** • DOI: 10.1021/acs.langmuir.5b03480 • Publication Date (Web): 21 Oct 2015

Cooling particle-coated bubbles: destabilization beyond dissolution arrest

Vincent Poulichet and Valeria Garbin*

Department of Chemical Engineering, Imperial College London, London SW7 2AZ, United Kingdom

E-mail: v.garbin@imperial.ac.uk

Abstract

Emulsions and foams that remain stable under varying environmental conditions are central in the food, personal care, and other formulated products industries. Foams stabilized by solid particles can provide longer-term stability than surfactant-stabilized foams. This stability is partly ascribed to the observation that solid particles can arrest bubble dissolution, which is driven by the Laplace pressure across the curved gas-liquid interface. We studied experimentally the effect of changes in temperature on the lifetime of particle-coated air microbubbles in water. We found that a decrease in temperature destabilizes particle-coated microbubbles beyond dissolution arrest. A quasi-steady model describing the effect of the change in temperature on mass transfer suggests that the dominant mechanism of destabilization is the increased solubility of the gas in the liquid, leading to a condition of undersaturation. Experiments at constant temperature confirmed that undersaturation alone can drive destabilization of particle-coated bubbles, even for vanishing Laplace pressure. We also found that dissolution of a particle-coated bubble can lead either to buckling of the coating, or

*To whom correspondence should be addressed

to gradual expulsion of particles, depending on the particle-to-bubble size ratio, with potential implications for controlled release.

Introduction

Foams stabilized by solid particles instead of molecular surfactants are exploited in food products and biomedical applications[1] and in advanced materials.[2,3] The stability imparted by solid particles has been shown to be much more effective than for the case for surfactants. Soluble surfactants only have a weak influence on the dissolution of gas bubbles, whereas insoluble surfactants such as proteins can considerably reduce the dissolution rate.[4,5] Whey protein isolate can prolong the lifetime of bubbles to just under an hour.[6] Class II hydrophobins can provide stability for at least few hours.[7] Monolayers of solid particles have been reported to stabilize bubbles for several days.[8] Solid particles adsorbed at the gas-liquid interface stabilize bubbles by preventing coalescence, disproportionation and dissolution.[9–13] A striking example of such stability is the dissolution arrest of particle-coated bubbles.[10]

Three main contributing factors have been identified for the stabilization of bubbles by surfactants or particles. Firstly, a decrease in surface tension γ helps prevent dissolution since the Laplace pressure, $\Delta P = 2\gamma/R$, decreases.[14,15] Secondly, an increased resistance to gas permeation is also invoked as a contribution to bubbles' stability,[4,16] and is particularly effective for high-molecular weight gases, such as perfluorocarbon.[17] Finally, the rheological properties of the interface contribute to the long term stability of coated bubbles. Theoretical calculations show that purely elastic interfaces can completely halt bubble dissolution, whereas interfacial viscosity alone is not sufficient to prevent dissolution.[18] For foams stabilized by solid particles, the elasticity of the interface has been reported to stop the dissolution, even if the surface tension is non-zero, provided that the elastic modulus ϵ satisfies $\epsilon > \gamma/2$.[19,20]

An additional argument, specific to particle-stabilized bubbles, has been put forward

to explain the observed dissolution arrest. The Laplace pressure can also decrease if the mean curvature of the interface decreases. In a certain range of particle-to-bubble size ratio, bubbles have been observed to become faceted, at which point dissolution stops. The dissolution arrest has been ascribed to the flattening of the interface located between particles in the monolayer, resulting in zero mean curvature.[10,21–23]

The effect of variations in temperature on the lifetime and durability of particle-stabilized drops and bubbles has not been investigated so far despite its importance for storage conditions of food and personal care products. Understanding the effect of cooling on stability could provide guidance for engineering stable particle-coated bubbles that are temperature resistant for prolonged shelf life and more versatile in applications.

In this paper, we report that particle-coated bubbles can be destabilized beyond dissolution arrest by a decrease in temperature. To understand this behavior, we also study the dissolution of uncoated bubbles with a time-dependent temperature, both in experiment and theory. We develop a simple model for uncoated bubble dissolution with time-dependent temperature, to isolate the effect of the different temperature-dependent parameters. The model reveals that the main mechanism that accelerates dissolution is the undersaturation of the external fluid caused by the increased gas solubility. The monolayer of particles can arrest dissolution due to the Laplace pressure, however it appears not to prevent dissolution in an undersaturated external phase. We also report different morphological transitions of the monolayer, including buckling and particle expulsion, depending on the particle-to-bubble size ratio.

Theory

Bubble dissolution at constant temperature

We first review the theory of bubble dissolution at constant temperature[24] including the effect of surface tension.[25] Mass transport across a gas-liquid interface occurs if the concentration

of gas in the liquid, c, is not the saturation concentration. The saturation concentration, c_s, is related to the partial pressure of gas acting on the liquid interface, P_g, through Henry's law:

$$c_s = k_H M P_g, \tag{1}$$

where k_H is the Henry's constant, which depends on the solubility of the gas in the liquid and is a function of temperature, and M the gas molar mass. Gas will diffuse into or out of the liquid, depending on whether $c < c_s$ or $c > c_s$, until equilibrium (saturation) is reached. The pressure of the gas inside a bubble is given by

$$P_g = P_0 + \frac{2\gamma}{R} \tag{2}$$

where P_0 is the ambient pressure at $r \to \infty$ and $\Delta P = 2\gamma/R$ the Laplace pressure caused by the curvature of the interface of a spherical bubble with radius R. We denote as $c_{s,0}$ the saturation concentration for a planar interface, $c_{s,0} = k_H M P_0$. As a consequence of Eq. (2), the saturation concentration in the liquid surrounding a bubble depends on the radius of the bubble, and bubbles can dissolve even if $c > c_{s,0}$. The driving force for dissolution due to the Laplace pressure is only pronounced for sufficiently small bubbles. For air bubbles in water at atmospheric pressure, $P_0 = 10^2$ kPa, with radius $R = 100$ μm, the Laplace pressure is $\Delta P \approx 1$ kPa, and the effect becomes negligible for larger bubbles.

The rate of change of radius of a bubble in a liquid can be obtained from a mass balance and the diffusion equation.[24] The rate of change of mass writes:

$$\frac{dm}{dt} = \frac{d}{dt}\left(\rho \frac{4}{3}\pi R^3\right) = 4\pi R^2 \left(\rho_0 + \frac{4M\gamma}{3R\,R_g T}\right)\dot{R} = -4\pi R^2 J, \tag{3}$$

where J is the outward mass flux of gas through the bubble's interface, and the overdot denotes derivative with respect to time. In Eq. (3) we have used the ideal gas law, $P_g =$

$\rho R_g T/M$, with R_g the gas constant, to express the gas density inside the bubble as:

$$\rho(R) = \rho_0 + \frac{M}{R_g T}\frac{2\gamma}{R}, \tag{4}$$

where $\rho_0 = \frac{P_0 M}{R_g T}$ is the density for a planar interface.

The mass flux, J, can now be related to the gas concentration gradient across the interface using Fick's second law. Assuming spherical symmetry, the gas concentration in the liquid at time t and at a distance r from the center of the bubble, $c(r,t)$, obeys:

$$\frac{\partial c}{\partial t} = D\Delta c = D\left(\frac{2}{r}\frac{\partial c}{\partial r} + \frac{\partial c}{\partial r^2}\right), \tag{5}$$

where D is the diffusion coefficient of the gas in the liquid. Inertial effects due to the motion of the bubble interface are neglected in Equation (5) because the interface motion due to gas diffusion is typically very slow.[24] Based on these simplifications, Epstein and Plesset[24] derived a solution that satisfies the following conditions:

$$c(r, t=0) = c_i,\ r > R, \tag{6}$$

$$\lim_{r\to\infty} c(r,t) = c_i,\ t > 0, \tag{7}$$

$$c(R,t) = c_s,\ t > 0, \tag{8}$$

where c_i denotes the initial concentration of gas in the solution. Equation (7) is verified when the volume of liquid is sufficiently large that the diffusion of gas from the bubble does not appreciably affect the concentration, c, except in the vicinity of the bubble. The concentration gradient across the bubble's interface is then:

$$\left.\frac{\partial c}{\partial r}\right|_{r=R} = (c_i - c_s)\left(\frac{1}{R} + \frac{1}{\sqrt{\pi D t}}\right). \tag{9}$$

The concentration gradient is related to the mass flux through Fick's first law:

$$J = -D \left. \frac{\partial c}{\partial r} \right|_{r=R}, \tag{10}$$

so that

$$J = -D(c_i - c_s) \left(\frac{1}{R} + \frac{1}{\sqrt{\pi D t}} \right). \tag{11}$$

Equations (3) and (11) are combined to express the rate of change in bubble radius:

$$\dot{R} = -\frac{D(c_s - c_i)}{\rho_0} \left(1 + \frac{2M}{3\rho_0 R_g T} \frac{2\gamma}{R} \right)^{-1} \left(\frac{1}{R} + \frac{1}{\sqrt{\pi D t}} \right). \tag{12}$$

Using Henry's law and assuming ideal gas behavior to express the saturation concentration in terms of Henry's constant, $c_s = \rho k_H R_g T$, Equation (12) can be recast as:

$$\dot{R} = -D k_H R_g T \left(1 - f + \frac{2M}{\rho_0 R_g T} \frac{2\gamma}{R} \right) \left(1 + \frac{2M}{3\rho_0 R_g T} \frac{2\gamma}{R} \right)^{-1} \left(\frac{1}{R} + \frac{1}{\sqrt{\pi D t}} \right). \tag{13}$$

We have separated out the dependence from $f = c_i/c_{s,0}$, the ratio between the initial concentration of dissolved gas and the saturation concentration for a planar interface. In practice, this is a parameter that can be independently controlled in experiment when preparing a solution with given dissolved gas concentration. Equation (13) shows how, even for $f = 1$, which corresponds to the equilibrium condition for a planar interface, the Laplace pressure $\Delta P = 2\gamma/R$ drives gas diffusion for a curved interface.

Bubble dissolution with time-dependent temperature

A time-dependent temperature, $T(t)$, affects the rate of bubble dissolution through the temperature dependence of several parameters. Firstly, the gas density inside the bubble depends on temperature through the ideal gas law, Equation (4). A decrease in temperature causes an increase in density, resulting in an increase in the saturation concentration following

Henry's law, and therefore an increase in rate of dissolution. Secondly, the surface tension increases with decreasing temperature,[26] typically as $\gamma \propto -T$, resulting in an increase in the Laplace pressure, which also causes faster dissolution. On the other hand, the diffusion coefficient decreases with temperature[27,28] as $D \propto T$, therefore slowing down dissolution. Finally, the solubility of the gas increases with decreasing temperature. This effect is reflected in the temperature dependence of the Henry's constant[29] as $k_H \propto \exp\left[C\left(\frac{1}{T}-\frac{1}{T_0}\right)\right]$, where C is a constant that depends on the gas, and T_0 is a reference temperature. The increase in solubility also causes faster dissolution. The interplay of these competing effects governs the rate of bubble dissolution with time-dependent temperature.

In the quasi-steady limit, Equation (9) can be assumed to be valid, and Equation (3) can be modified to account for a time-dependent temperature:

$$\begin{aligned}\frac{dm}{dt} =& \frac{d}{dt}\left\{\left(\frac{P_0 M}{BT}+\frac{2M\gamma}{BTR}\right)\frac{4}{3}\pi R^3\right\}\\ =& 4\pi R^2\left[\left(\rho_0+\frac{4M\gamma}{3R\,R_g T}\right)\dot{R}-\left(\frac{P_0 MR+2M\gamma}{3R_g T^2}+\frac{2M}{3BT}\frac{d\gamma}{dT}\right)\dot{T}\right];\end{aligned} \tag{14}$$

Equation 13 is then modified with a term proportional to the cooling rate $\dot{T}$:

$$\begin{aligned}\dot{R} =& -D\,k_H R_g T\left(1-f+\frac{2M\gamma}{R\rho_0 R_g T}\right)\left(1+\frac{4M\gamma}{3\rho_0 R R_g T}\right)^{-1}\left(\frac{1}{R}+\frac{1}{\sqrt{\pi D t}}\right)\\ &+\dot{T}\left(\frac{\frac{BT\rho_0}{M}R+2\gamma+2T\frac{d\gamma}{dT}}{3T(\frac{BT\rho_0}{M}+\frac{4\gamma}{3R})}\right).\end{aligned} \tag{15}$$

We implement the temperature dependence of the diffusion coefficient D,[27,28] the surface tension γ,[30] and the Henry's constant k_H,[29] according to the following relations:

$$\begin{aligned}\frac{D\eta}{T} &= \text{constant},\\ \text{with } \eta &= \eta_0 \exp\left[aP_0+\frac{E-bP_0}{R_g(T-\theta_g-cP_0)}\right]\end{aligned} \tag{16}$$

the temperature dependence of water viscosity, where $R_g = 8.314$ J K^{-1} mol^{-1} is the ideal

gas constant, and $\eta_0 = 2.4055 \times 10^{-5}$ Pa s, $E = 4.753$ kJ/mol, $\theta_g = 139.7$ K, $a = 44.2$ Pa^{-1}, $b = 9.565 \times 10^{-9}$ kJ mol^{-1} Pa^{-1}, $c = 1.24 \times 10^{-7}$ K/Pa;

$$\gamma = B \left[\frac{T_c - T}{T_c}\right]^{\mu} \left[1 + d\left(\frac{T_c - T}{T_c}\right)\right], \tag{17}$$

where $T_c = 647.15$ K is the critical temperature of water, and the parameters in the correlation are $B = 235.8$ mN/m, $d = -0.625$, $\mu = 1.256$;

$$k_H = k_H(T_0)\, \exp\left[C\left(\frac{1}{T} - \frac{1}{T_0}\right)\right], \tag{18}$$

with $k_H(T_0) = 6.4 \times 10^{-6}$ mol m^{-3} Pa^{-1} the value of the Henry's constant for nitrogen at the reference temperature $T_0 = 298.15$ K, and the constant $C = 1500$ K for nitrogen. The general solution of the temperature-dependent problem, including unsteady effects, requires solving Equation (5) with a time-dependent diffusion coefficient, and treating the boundary condition in Equation (8) as time-dependent. The quasi-steady approximation is satisfactory for the system considered, since the timescale for the change in temperature ($t_f \sim 10^2$ s) is slower than the characteristic timescale for bubble dissolution, $\tau_D \approx R^2/D \sim 10$ s. This simplified model is used to provide a qualitative understanding of the role of the different temperature-dependent parameters on bubble dissolution.

Effect of decrease in temperature on bubble dissolution

To investigate the effect of a decrease in temperature on bubble dissolution, we solve Equation (15) numerically, with the initial condition $R(t = 0) = R_0$. The temperature T is a time-dependent coefficient, and the other time-dependent coefficients, D, γ, and k_{H}, are given by Equations (16-18). The temperature decreases linearly from $T_0 = 298$ K at $t = 0$, to a final temperature T_f at $t = t_f$. The initial values of the temperature-dependent parameters are $D(T_0) = 1 \times 10^{-9}$ m^2 s^{-1} and $f(T_0) = 1$. The other constants are the atmospheric pressure $P_0 = 10^5$ Pa, the density of water $\rho_0 = 1000$ kg m^{-3}, and the molar mass of nitrogen

$M = 28.96 \times 10^{-3}$ kg mol^{-1}.

We investigate the effects of the change in temperature, $\Delta T = T_f - T_0$, and of the rate of change of temperature, $\dot{T} = \frac{T_f - T_0}{t_f}$. Figure 1a shows the temporal evolution of the

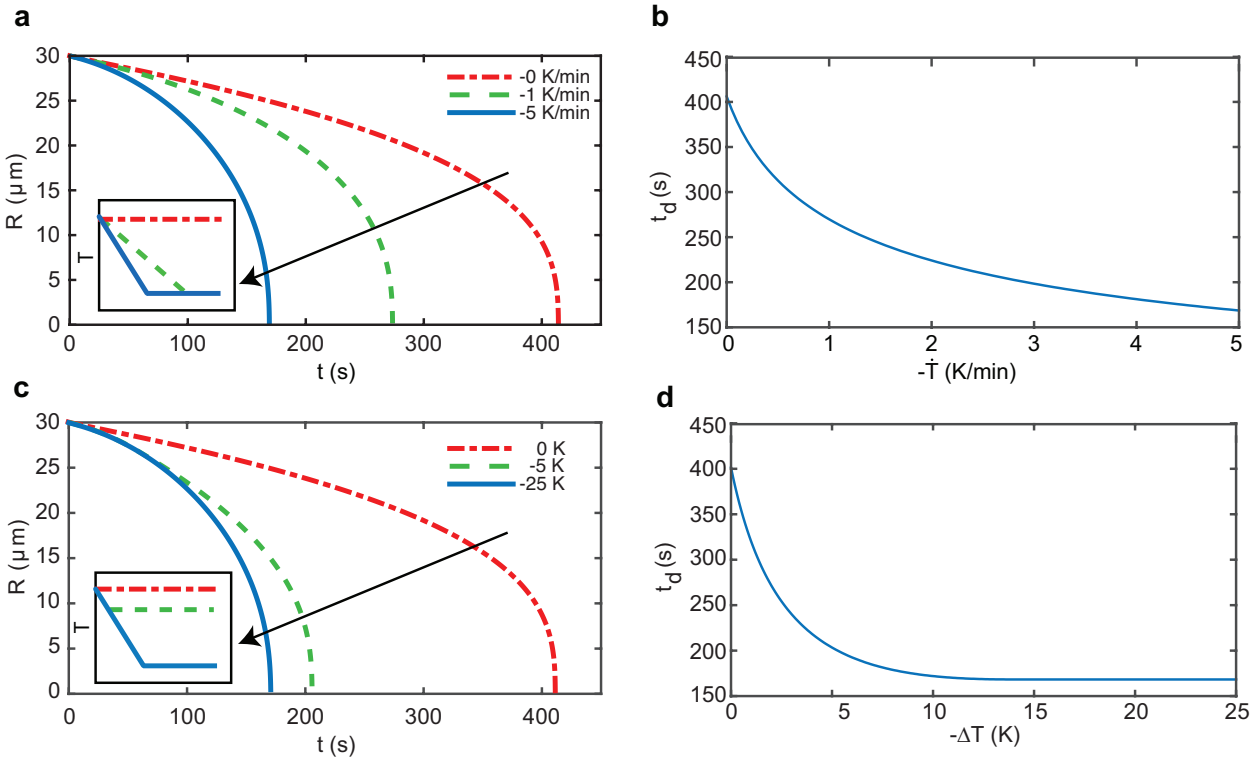

Figure 1: Influence of cooling rate $\dot{T}$ and change in temperature ΔT on the dissolution rate of uncoated bubbles. (a) Time evolution of the radius for different cooling rates and the same change in temperature (see inset). (b) Dependence of the time to dissolution t_d on the cooling rate. (c) Time evolution of the radius for different changes in temperature at the same cooling rate (see inset). (d) The dependence of the time to dissolution t_d on the change in temperature.

radius of a dissolving bubble with initial radius $R_0 = 30$ μm. For constant temperature, the characteristic behavior is observed, with the rate of change of radius rapidly increasing with decreasing bubble size. The time to dissolution is $t_d \approx 410$ s. When the system is cooled down to $T_f = 273$ K, the time to dissolution decreases with increasing cooling rate, $t_d \approx 270$ s for $\dot{T} = -1$ K/min, and $t_d \approx 170$ s for $\dot{T} = -5$ K/min. Figure 1b reports the nonlinear dependence of the time to dissolution in the range of cooling rates accessible in experiment. The time to dissolution for a fixed cooling rate $\dot{T} = -5$ K/min and different

change in temperature ($\Delta T = 0$ K, -5 K, -25 K) is shown in Figure 1c. The dependence of the time to dissolution, t_d, on the change in temperature is strongly nonlinear, with a dramatic decrease for $\Delta T = -5$ K, and only a small difference between $\Delta T = -5$ K and $\Delta T = -25$ K, as shown also in Figure 1d.

To identify the main driving force for the increased rate of dissolution, we isolate the effect of each of the temperature-dependent parameters. Figure 2 shows that the increase in

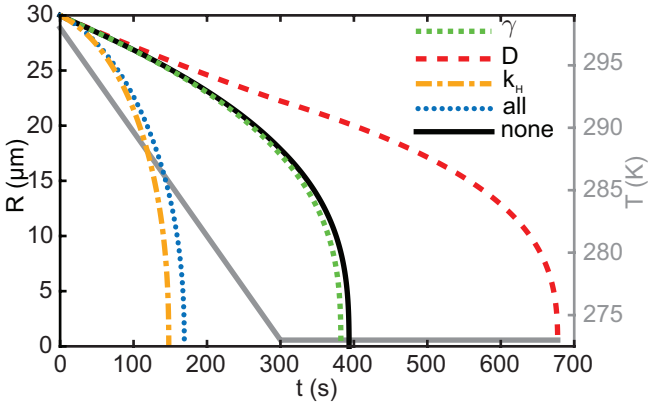

Figure 2: Effect of the individual temperature-dependent parameters on the dissolution dynamics of a bubble. The time dependence of the temperature is also shown.

surface tension increases the rate of dissolution only slightly. On the other hand, the decrease in diffusion coefficient significantly decreases the rate of dissolution. Lastly, the increase in Henry's constant causes a significant increase in the dissolution rate. The dissolution curve obtained by taking into account the temperature dependence of all three parameters suggests that the increase in gas solubility upon cooling is the main contribution to the increase in dissolution rate. The increase in k_H causes an increase in the saturation concentration, $c_{s,0} = \rho_0 k_H R_g T$, and therefore a decrease in the saturation f. For an initially saturated solution, $f = 1$ at $T_0 = 298$ K, a change in temperature $\Delta T = -25$ K results in an undersaturation $f \approx 0.6$. Undersaturation of the external phase drives the dissolution of drops and bubbles even if the Laplace pressure vanishes, as shown by Equation (13). Undersaturation is typically achieved by diluting the external phase.[31] Here the external phase becomes unsaturated solely because of the increase in gas solubility upon cooling.

Experimental Methods

Particle-stabilized bubbles

Charge-stabilized, hydrophilic polystyrene beads (Life Technologies, Invitrogen) were suspended in a solution of 500 mM NaCl (BioXtra, Sigma-Aldrich) in ultrapure water with resistivity 18.2 MΩ cm (Milli-Q filtration system, Millipore). The particle diameters used are $2a = 0.5$ μm, $2a = 3.1$ μm, and $2a = 5$ μm. Particle-coated bubbles were formed by mechanical agitation using a vortex mixer. Particle-stabilized bubbles were resuspended in NaCl solution and placed in an observation chamber made of a microscope glass slide and a coverslip separated by a spacer. All NaCl solutions were equilibrated at room temperature and atmospheric pressure to obtain a saturation $f \approx 1$, unless otherwise stated.

Cooling experiments

The observation chamber was placed in a temperature controlled stage (THMS600, Linkam). The rate of cooling and the final cooling temperature were set using the provided software Linksys32. Images were recorded every 15 seconds with a camera mounted on a upright reflection microscope (Olympus) with 10× magnification.

Undersaturation experiments

The setup consists in a closed container of volume 2.2 mL, with an inlet for introducing degassed liquid and an outlet, placed on the microscope stage. The inlet is connected to a syringe pump (Harvard Apparatus). The degassed solution is prepared by placing a beaker of the NaCl solution in a vacuum chamber held at -1 bar for at least 24 hours. The container is initially filled with saturated solution, in which particle-coated bubbles remain stable. The concentration of dissolved gas in the external phase is then reduced by injecting 2.025 mL of degassed solution at a constant flow rate of 5 μL/min, so as to replace the external phase. The flow rate is sufficiently small that the bubble remains in the field of view of the

microscope.

Experimental Results

We compared the dissolution behavior of uncoated and particle-stabilized bubbles. Figures 3(a-b) show the dramatic increase in dissolution rate of uncoated bubbles upon cooling, in keeping with the predictions of the model. In all cases the solution is initially saturated with gas, i.e., $c \approx c_{s,0}$, or $f \approx 1$. In Figure 3a, a bubble with initial radius $R_0 \approx 10$ μm dissolves at constant temperature over a time $t_d \approx 850$ s. A larger bubble, with initial radius $R_0 \approx 30$ μm, that is cooled by $\Delta T = -17$ K at a rate $\dot{T} = -5$ K/min dissolves over the same time scale, *i.e.*, at a faster rate. The time over which the temperature decreases is $t_f = 300$ s. In contrast to the behavior of an uncoated bubble dissolving at constant temperature, a particle-stabilized bubble remains stable. Figure 3c shows no change in radius of a bubble with initial radius $R_0 \approx 15$ μm over a timescale of more than 10^3 s.

Since the Laplace pressure, $\Delta P = 2\gamma/R$, is the only driving force for dissolution in a saturated solution ($f = 1$), the stability of the particle-coated bubble is due either to the elasticity of the monolayer, which can prevent dissolution provided that the elastic modulus satisfies $\epsilon > \gamma/2$,[19,20] or to the flattening of the interface that makes the Laplace pressure vanish.[10,21–23] The surface elastic modulus of the colloid monolayer (3-μm particles) is $\epsilon \approx 20$ mN/m, as measured in a Langmuir trough compression experiment.[32] The effective surface tension of the particle-laden gas/water interface would need to be $\gamma \lesssim 40$ mN/m for the above stability criterion to be satisfied. This surface tension corresponds to a fractional area coverage $\phi \approx 0.6$, as obtained from optical microscopy on the Langmuir trough.[32] These values seem reasonable since they are well below the threshold for collapse and buckling, which on the Langmuir trough occurs at $\gamma \approx 20$ mN/m for $\phi \approx 0.7$. In stark contrast with the stability observed at constant temperature, a particle-coated bubble dissolves completely upon cooling (Figure 3d). The bubble changes morphology during dissolution: it becomes

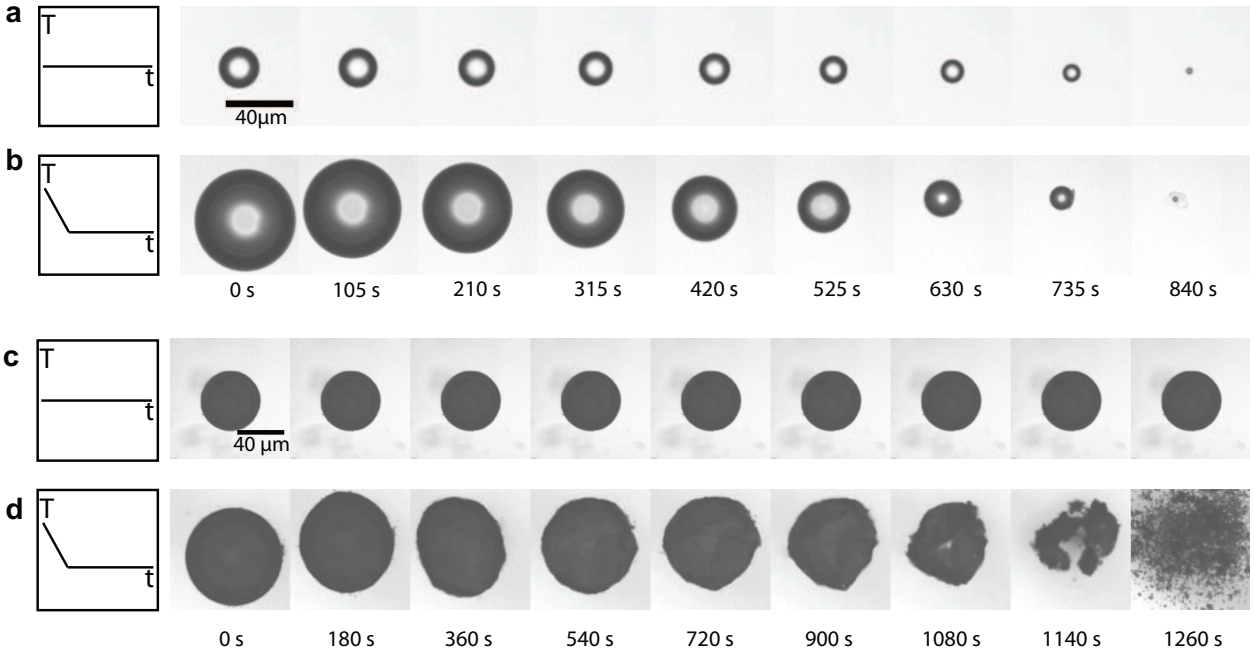

Figure 3: Effect of a decrease in temperature on the dissolution of uncoated and particle-stabilized bubbles. (a) Uncoated bubble dissolving at constant temperature. (b) Uncoated bubble dissolution is enhanced by a decrease in temperature $\Delta T = -17$ K. (c) Bubble coated by 3-μm particles remains stable at constant temperature. (d) Particle-coated bubble is destabilized by a decrease in temperature and completely dissolves. The timescales in the temperature profiles are not to scale.

non-spherical ($t = 360$ s), its interface buckles ($t = 720$ s), and it eventually breaks up into multiple non-spherical bubbles ($t = 1080$ s). During this process, particles detach from the coating, and they sediment to the bottom of the observation chamber ($t = 1260$ s).

Figure 4 compares the time evolution of the radii of uncoated bubbles for the two cases of constant temperature and $\dot{T} = -5$ K/min. The behaviour observed experimentally agrees qualitatively with that of the model: cooling bubbles results in a strong increase in their dissolution rate. The results of the model for bubble dissolution are not directly comparable

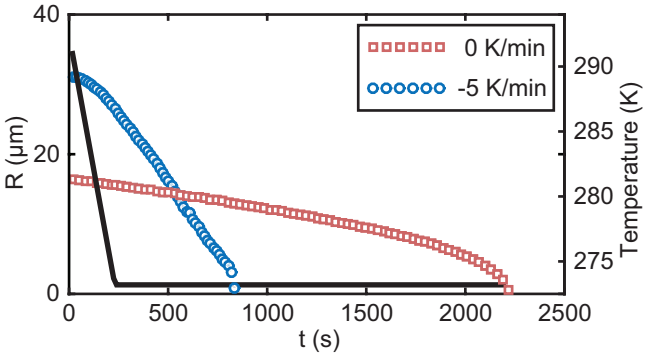

Figure 4: Time evolution of the radius of two uncoated bubbles obtained from experiments at constant temperature (squares) and with cooling (circles). The temperature profile for the cooling experiment is also shown.

with the experimental results. Firstly, the model is derived in the steady-state limit. In addition, the assumption was made of an unbounded fluid. However, in experiment the bubbles come into contact with a solid boundary because of buoyancy, and therefore their dissolution behavior is affected by confinement, which considerably slows down the process.[33] Particle-stabilized bubbles become non-spherical and break up upon dissolution, so it was not possible to track their radius (see Figure 3d).

We performed an experiment in which we decreased the dissolved gas concentration at constant temperature, and confirmed that the main driving force for the enhanced dissolution of cooled bubbles is the undersaturation of the external phase (Figure 5). We slowly added undersaturated solution in the chamber containing particle-coated bubbles suspended in an initially saturated external phase. The bubbles are stable in the saturated liquid, as

already shown in Figure 3c. Upon addition of undersaturated solution, the coated bubble is noticeably smaller when the concentration of air in the external phase has reached an undersaturation $f \approx 0.7$ ($t = 135$ s). The subsequent dissolution of the particle-coated bubble is shown until ($t = 360$ s). This result is analogous to the behavior of nanoparticle-coated droplets of partially miscible liquid made in an initially saturated external phase, which dissolve and crumple upon dilution of the external phase with unsaturated liquid.[31] We also verified that particle-coated bubbles initially made at low temperature are stable at constant temperature (data not shown). It was possible to make particle-coated bubbles with a saturated solution at 277 K. Note that the saturation concentration at 277 K is higher than at room temperature. The solution was left to equilibrate at 277 K to achieve saturation concentration before the bubbles were made. This observation confirms that the enhanced dissolution of particle-coated bubble does not spontaneously occur at low temperature. Rather, the decrease in temperature, and resulting increase in gas solubility, destabilizes bubbles that were initially stable in a saturated solution.

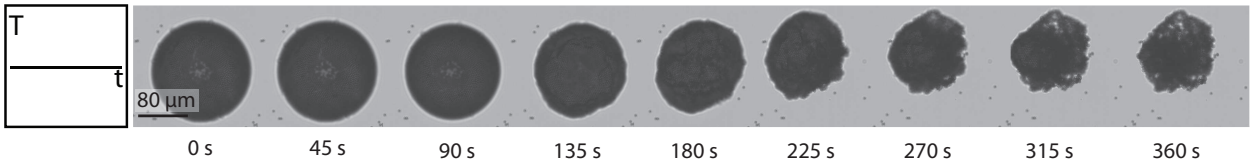

Figure 5: Destabilization and dissolution of particle-coated bubble driven by undersaturation ($f < 1$) of the external phase.

We observed different morphological transitions in the particle monolayer during bubble dissolution, depending on the ratio between particle radius and bubble radius, a/R, as shown in Figure 6. The rate of cooling is $\dot{T} = -5$ K/min and the change in temperature $\Delta T = 17$ K for all the experiments shown. By changing both the particle size ($a = 0.25, 1.55, 2.5$ μm) and the bubble size ($R \approx 50 - 200$ μm), we explored the range of particle-to-bubble size ratio $a/R \sim 10^{-3} - 10^{-1}$. Figure 6a shows the dissolution of a particle-coated bubble with $a/R \approx 1.2 \times 10^{-3}$. The interface first exhibits one large in-

ward buckling of the scale of R (t = 1350 s), while the bubble takes an elongated shape, also observed during the dissolution of lipid-coated microbubbles[14] and nanoparticle-coated droplets.[31] After further dissolution, the interface shows secondary wrinkles of smaller length scale (t = 5400 s). Finally, when the bubble has completely dissolved, the monolayer collapses forming a skin of particles, again similar to the behavior reported for nanoparticle-coated droplets,[31] and deflating microparticle-coated drops.[34] For larger particle-to-bubble size ratio, $a/R \approx 1.5 \times 10^{-2}$, shown in Figure 6b, the bubble also takes an elongated shape upon initial dissolution (t = 315 s), with a buckling of the scale of R. The bubble then breaks up into smaller bubbles (t = 735 s), which completely dissolve. In contrast with the previous example, at the end of the process all the particles have been released from the monolayer, and have sedimented at the bottom of the observation chamber (t = 945 s). As the particle-

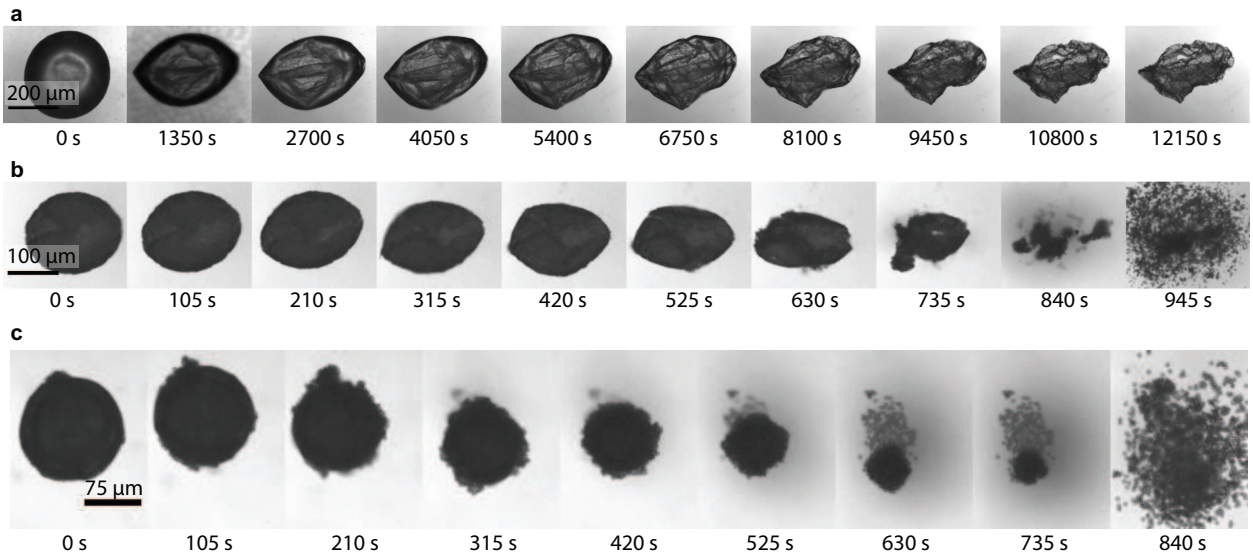

Figure 6: Dissolution of particle-stabilized bubbles induced by a decrease in temperature for different particle-to-bubble size ratios. (a) The particle monolayer forms a skin for $a/R \approx 1.2 \times 10^{-3}$. (b) The monolayer buckles and expels particles for $a/R \approx 1.5 \times 10^{-2}$. (c) The bubble becomes faceted and particles are expelled from the monolayer for $a/R \approx 3 \times 10^{-2}$.

to-bubble size ratio is further increased, $a/R \approx 3 \times 10^{-2}$ (Figure 6c), a different behavior is observed. The bubble exhibits buckling on the scale of a fraction of R (t = 210 s), and looks faceted when the particle-to-bubble size ratio has decreased to $a/R \sim 10^{-1}$ (t = 525 s). Particles desorb continuously from the air-water interface and sediment at the bottom of the

observation chamber ($t = 840$ s). Buckling followed by expulsion of the coating material was suggested to occur during the dissolution of bubbles stabilized by fluorinated surfactants,[35] although expulsion could not be directly visualized.

The effect of particle-to-bubble size ratio on the morphology of deflating armored drops has recently been investigated in conjunction with measurements of collapse pressure.[36] The morphology changes from wrinkled or buckled, to faceted, with increasing value of a/R. In contrast with the results of Ref. [36], in our experiments we also observe shedding of particles for the larger particle-to-bubble size ratios ($a/R > 10^{-2}$). This difference can be ascribed to the different wettability of the particles used, since we used hydrophilic particles, while hydrophobic particles were used in Ref. [36]. For flat monolayers compressed on a Langmuir trough, the collapse scenario has been shown to depend on wettability because of the different microstructures formed at the interface.[37] More hydrophilic particles form a liquid-like monolayer and, upon area compression, they are expelled in the aqueous subphase. For more hydrophobic particles, a cohesive monolayer is formed, which buckles like a solid film upon compression. Since in our system the particles are hydrophilic, and the curvature of the interface facilitates outward expulsion of particles, redispersion of particles in the external phase is favorable, unlike in Ref. [36].

Conclusions

We studied the effect of a decrease in temperature on the stability of particle-coated bubbles. Particle-coated bubbles exhibit outstanding stability because the elasticity of the monolayer can counter the effect of the Laplace pressure, or owing to a vanishing Laplace pressure for the particular case of faceted bubbles. Strikingly, we found that particle-stabilized air bubbles dissolve completely in water upon cooling. Experiments on uncoated bubbles show that the decrease in temperature accelerates bubble dissolution as compared to constant temperature. To explain why this enhanced dissolution is also observed for particle-stabilized

bubbles, we developed a quasi-steady model of uncoated bubble dissolution and evaluated the effect of the different temperature-dependent parameters. The model suggests that the dominant contribution to enhanced dissolution is the increase in gas solubility with decreasing temperature, which results in the undersaturation of the external phase. This mechanism was confirmed in an experiment at constant temperature, in which the saturated external phase was diluted with unsaturated solution, causing initially stable particle-coated bubbles to dissolve. The destabilization of particle-coated bubbles is therefore caused by the undersaturation of the external phase. While the monolayer of particles can counter the driving force for dissolution due to the Laplace pressure, it cannot prevent dissolution in an undersaturated external phase. The morphological transitions observed for dissolving particle-coated bubbles range from wrinkled or buckled to faceted, depending on the particle-to-bubble size ratio. After complete bubble dissolution, the particle monolayer is found to form a crumpled skin for particle-to-bubble size ratio smaller than $\sim 10^{-2}$, whereas particles are slowly released from dissolving bubbles having a larger particle-to-bubble size ratio . The observation of destabilization of particle-coated bubbles by cooling has implications for the design of formulated products that remain stable under varying environmental conditions. Temperature-triggered expulsion of particles from dissolving bubbles or drops can also be exploited in controlled release applications.

Acknowledgement

The authors thank Y. Chi for performing preliminary experiments, B. Dollet and A. G. Marín for helpful discussions, and J. T. Cabral for access to the temperature controlled stage.

References

(1) Lam, S.; Velikov, K. P.; Velev, O. D. Pickering stabilization of foams and emulsions with particles of biological origin. *Current Opinion in Colloid & Interface Science* **2014**, *19*, 490 – 500.

(2) Zhang, Y.; Allen, M. C.; Zhao, R.; Deheyn, D. D.; Behrens, S. H.; Meredith, J. C. Capillary foams: stabilization and functionalization of porous liquids and solids. *Langmuir* **2015**, *31*, 2669–2676.

(3) Zhang, Y.; Wu, J.; Wang, H.; Meredith, J. C.; Behrens, S. H. Stabilization of liquid foams through the synergistic action of particles and an immiscible liquid. *Angewandte Chemie* **2014**, *126*, 13603–13607.

(4) Hanwright, J.; Zhou, J.; Evans, G. M.; Galvin, K. P. Influence of surfactant on gas bubble stability. *Langmuir* **2005**, *21*, 4912–4920.

(5) Soetanto, K.; Chan, M.; Okujima, M. Change in size and number of sodium laurate microbubbles with time in saline at different air concentrations. *Japanese Journal of Applied Physics* **1997**, *36*, 3238.

(6) Dickinson, E.; Ettelaie, R.; Murray, B. S.; Du, Z. Kinetics of disproportionation of air bubbles beneath a planar air–water interface stabilized by food proteins. *Journal of Colloid and Interface Science* **2002**, *252*, 202–213.

(7) Cox, A. R.; Cagnol, F.; Russell, A. B.; Izzard, M. J. Surface properties of class II hydrophobins from Trichoderma reesei and influence on bubble stability. *Langmuir* **2007**, *23*, 7995–8002.

(8) Du, Z.; Bilbao-Montoya, M. P.; Binks, B. P.; Dickinson, E.; Ettelaie, R.; Murray, B. S. Outstanding stability of particle-stabilized bubbles. *Langmuir* **2003**, *19*, 3106–3108.

(9) Dickinson, E.; Ettelaie, R.; Kostakis, T.; Murray, B. S. Factors controlling the formation and stability of air bubbles stabilized by partially hydrophobic silica nanoparticles. *Langmuir* **2004**, *20*, 8517–8525.

(10) Abkarian, M.; Subramaniam, A. B.; Kim, S.-H.; Larsen, R. J.; Yang, S.-M.; Stone, H. A.

Dissolution arrest and stability of particle-covered bubbles. *Physical Review Letters* **2007**, *99*, 188301.

(11) Park, J. I.; Nie, Z.; Kumachev, A.; Abdelrahman, A. I.; Binks, B. P.; Stone, H. A.; Kumacheva, E. A microfluidic approach to chemically driven assembly of colloidal particles at gas–liquid interfaces. *Angewandte Chemie* **2009**, *121*, 5404–5408.

(12) Rodrigues, J. A.; Rio, E.; Bobroff, J.; Langevin, D.; Drenckhan, W. Generation and manipulation of bubbles and foams stabilised by magnetic nanoparticles. *Colloids and Surfaces A: Physicochemical and Engineering Aspects* **2011**, *384*, 408–416.

(13) Tumarkin, E.; Park, J. I.; Nie, Z.; Kumacheva, E. Temperature mediated generation of armoured bubbles. *Chemical Communications* **2011**, *47*, 12712–12714.

(14) Borden, M. A.; Longo, M. L. Dissolution behavior of lipid monolayer-coated, air-filled microbubbles: Effect of lipid hydrophobic chain length. *Langmuir* **2002**, *18*, 9225–9233.

(15) Pu, G.; Borden, M. A.; Longo, M. L. Collapse and shedding transitions in binary lipid monolayers coating microbubbles. *Langmuir* **2006**, *22*, 2993–2999.

(16) Katiyar, A.; Sarkar, K.; Jain, P. Effects of encapsulation elasticity on the stability of an encapsulated microbubble. *Journal of Colloid and Interface Science* **2009**, *336*, 519–525.

(17) Sarkar, K.; Katiyar, A.; Jain, P. Growth and dissolution of an encapsulated contrast microbubble: effects of encapsulation permeability. *Ultrasound in Medicine & Biology* **2009**, *35*, 1385–1396.

(18) Kloek, W.; van Vliet, T.; Meinders, M. Effect of bulk and interfacial rheological properties on bubble dissolution. *Journal of Colloid and Interface Science* **2001**, *237*, 158–166.

(19) Stocco, A.; Rio, E.; Binks, B. P.; Langevin, D. Aqueous foams stabilized solely by particles. *Soft Matter* **2011**, *7*, 1260–1267.

(20) Murray, B. S.; Ettelaie, R. Foam stability: proteins and nanoparticles. *Current Opinion in Colloid & Interface Science* **2004**, *9*, 314–320.

(21) Johnson, B. D.; Wangersky, P. J. Microbubbles: Stabilization by monolayers of adsorbed particles. *Journal of Geophysical Research: Oceans (1978–2012)* **1987**, *92*, 14641–14647.

(22) Kam, S. I.; Rossen, W. R. Anomalous capillary pressure, stress, and stability of solids-coated bubbles. *Journal of Colloid and Interface Science* **1999**, *213*, 329–339.

(23) Subramanian, R. S.; Larsen, R. J.; Stone, H. A. Stability of a flat gas-liquid interface containing nonidentical spheres to gas transport: Toward an explanation of particle stabilization of gas bubbles. *Langmuir* **2005**, *21*, 4526–4531.

(24) Epstein, c. e. P.; Plesset, M. On the Stability of Gas Bubbles in Liquid-Gas Solutions. *The Journal of Chemical Physics* **1950**, *18*, 1505–1509.

(25) Duncan, P. B.; Needham, D. Test of the Epstein-Plesset model for gas microparticle dissolution in aqueous media: Effect of surface tension and gas undersaturation in solution. *Langmuir* **2004**, *20*, 2567–2578.

(26) Guggenheim, E. A. The principle of corresponding states. *The Journal of Chemical Physics* **1945**, *13*, 253–261.

(27) Krynicki, K.; Green, C. D.; Sawyer, D. W. Pressure and temperature dependence of self-diffusion in water. *Faraday Discussions of the Chemical Society* **1978**, *66*, 199–208.

(28) Likhachev, E. Dependence of water viscosity on temperature and pressure. *Technical Physics* **2003**, *48*, 514–515.

(29) Sander, R. Compilation of Henry's law constants, version 3.99. *Atmospheric Chemistry and Physics Discussions* **2014**, *14*, 29615–30521.

(30) Vargaftik, N.; Volkov, B.; Voljak, L. International tables of the surface tension of water. *Journal of Physical and Chemical Reference Data* **1983**, *12*, 817–820.

(31) Datta, S. S.; Shum, H. C.; Weitz, D. A. Controlled buckling and crumpling of nanoparticle-coated droplets. *Langmuir* **2010**, *26*, 18612–18616.

(32) Poulichet, V.; Garbin, V. Ultrafast desorption of colloidal particles from fluid interfaces. *Proceedings of the National Academy of Sciences* **2015**, *112*, 5932–5937.

(33) Kentish, S.; Lee, J.; Davidson, M.; Ashokkumar, M. The dissolution of a stationary spherical bubble beneath a flat plate. *Chemical Engineering Science* **2006**, *61*, 7697–7705.

(34) Monteux, C.; Kirkwood, J.; Xu, H.; Jung, E.; Fuller, G. G. Determining the mechanical response of particle-laden fluid interfaces using surface pressure isotherms and bulk pressure measurements of droplets. *Physical Chemistry Chemical Physics* **2007**, *9*, 6344–6350.

(35) Kovalenko, A.; Polavarapu, P.; Pourroy, G.; Waton, G.; Krafft, M. P. pH-Controlled microbubble shell formation and stabilization. *Langmuir* **2014**, *30*, 6339–6347.

(36) Pitois, O.; Buisson, M.; Chateau, X. On the collapse pressure of armored bubbles and drops. *The European Physical Journal E* **2015**, *38*, 1–7.

(37) Razavi, S.; Cao, K. D.; Lin, B.; Lee, K. Y. C.; Tu, R. S.; Kretzschmar, I. Collapse of Particle-Laden Interfaces under Compression: Buckling vs Particle Expulsion. *Langmuir* **2015**, *31*, 7764–7775.

Graphical TOC Entry